Characterization of Mitochondrial Metabolism in L6 Rat Myoblasts

by
Emily Burney

A THESIS

submitted to

Oregon State University

Honors College

in partial fulfillment of
the requirements for the
degree of

Honors Baccalaureate of Science in Public Health
(Honors Scholar)

Presented June 8, 2018
Commencement June 2018

AN ABSTRACT OF THE THESIS OF

Emily Burney for the degree of Honors Baccalaureate of Science in Public Health presented on June 8, 2018. Title: Characterization of Mitochondrial Metabolism in L6 Rat Myoblasts

Abstract approved:_____

Matthew Robinson

The prevalence of obesity is increasing worldwide, causing a subsequent increase in insulin resistance (IR), metabolic disorders, and cardiovascular diseases. Although these conditions significantly impact both the individual and society, their etiologies have not been discovered, inhibiting potential prevention and treatment. Alterations to mitochondrial metabolism are implicated in the development of IR and progression to Type 2 Diabetes (T2D), raising the need for an investigation of mitochondrial metabolism in skeletal muscle. Understanding metabolism on an individual substrate basis within a model system enables identification of each nutrient's contribution to respiration and potential mitochondrial dysfunction. As such, the purpose of this investigation was to characterize mitochondrial metabolism and determine mitochondrial respiratory control in L6 rat myoblasts. High-resolution respirometry and three Substrate-Uncoupler-Inhibitor-Titration (SUIT) protocols were used to examine respiration. Mitochondrial capacity was not limited by the electron transfer system, although the presence of multiple substrates potentially flooded the Q-junction, resulting in lower respiratory control and indicating the presence of a potential limiting factor. In sum, L6 myoblasts exhibit no overt defects in mitochondrial metabolism, but may have a propensity for substrate overload, thereby limiting respiration.

Key Words: Mitochondria, L6 myoblasts, oxidative phosphorylation, electron transfer

Corresponding e-mail address: burney.emily@gmail.com

Characterization of Mitochondrial Metabolism in L6 Rat Myoblasts

by
Emily Burney

A THESIS

submitted to

Oregon State University

Honors College

in partial fulfillment of
the requirements for the
degree of

Honors Baccalaureate of Science in Public Health
(Honors Scholar)

Presented June 8, 2018
Commencement June 2018

Honors Baccalaureate of Science in Public Health project of Emily Burney presented on June 8, 2018.

APPROVED:

_____

Matthew Robinson, Mentor, representing Biological and Population Health Sciences

_____

Sean Newsom, Committee Member, representing Biological and Population Health Sciences

_____

Indira Rajagopal, Committee Member, representing Biochemistry and Biophysics

_____

Toni Doolen, Dean, Oregon State University Honors College

I understand that my project will become part of the permanent collection of Oregon State University, Honors College. My signature below authorizes release of my project to any reader upon request.

_____

Emily Burney, Author

INTRODUCTION

Insulin Resistance Negatively Impacts Health

Over 60% of American adults are overweight or obese and 14% of children and 12% of adolescents are overweight. These numbers have doubled since the 1980s (33). As obesity rates increase, so does the prevalence of insulin resistance (IR), and correspondingly, the importance of this public health concern. Insulin resistance can be defined as a subnormal cellular response to the normal actions of insulin (31). Studies have shown a causal link between IR and weight gain, although not all forms of obesity lead to IR (12). Despite this inconsistency, insulin resistance has a detrimental impact throughout the body, causing aberrant nutrient partitioning, accumulation of metabolites, and disorder in endocrine tissue (18). It mediates risk for many metabolic diseases, including cardiovascular diseases and Type 2 Diabetes (T2D) (a condition characterized by insulin resistance) so it is unsurprising that the ongoing obesity pandemic has given rise to a secondary increase in the incidence and prevalence of T2D (29). In addition, over 84 million adults in the United States (more than 1 out of 3) are currently estimated to have prediabetes, another metabolic disease state characterized by insulin resistance (25). The impact of insulin resistance may even extend beyond metabolic disorders and cardiovascular disease, with a study showing that insulin resistant, non-diabetic patients had as high a risk of developing late onset Alzheimer's Disease as patients with the genetic risk factors (15).

The impact of obesity, insulin resistance, and metabolic and cardiovascular diseases extends beyond an individual's metabolic health. In 2017, 24.7 million people (9.7% of the adult population) in the U.S. were diagnosed with T2D. The estimated national cost of this disease was $327 billion, and approximately 1 in 4 of all health care dollars spent is spent on health care costs incurred by those with diabetes (1). In addition, 65 million more adults are projected to be

obese by 2030, resulting in further increases in cases of diabetes, cardiovascular disease, and quality-adjusted life years lost, as well as an increase in medical costs related to these diseases of $48-66 billion per year (32). These costs can be expected to grow further as obesity rates increase, since on average worldwide obese individuals incur obesity-related medical costs that are 30% greater than those of their lean peers (16). Even without diagnosed metabolic health issues, non-diabetic patients with higher levels of fasting plasma glucose (FPG), which indicates insulin resistance and abnormal glucose metabolism, were shown to have over $1000 higher medical care costs than peers with normal FPG annually (20). Potential solutions for the prevention and management of obesity include diet and exercise, pharmacological therapies, surgical interventions, and behavioral modification, but no method has been able to satisfactorily address the complex multifactorial aspects of obesity and related health conditions. The current treatment of these conditions amounts to nearly 10% of the US healthcare budget (7). Overall, the morbidity, mortality, and the associated economic burden attributable to insulin resistance is significant.

Given the prevalence of T2D and prediabetes, among the myriad of other related issues noted above, the occurrence of insulin resistance sounds an alarm for those hoping to prevent it from progressing to T2D and other related co-morbidities. However, while the presence of IR signals the beginning of a slippery slope, there is a lack of conclusive evidence for effective prevention or treatment options. In one study, lifestyle and metformin-based interventions improved insulin sensitivity independent of the presence of established genetic determinants for IR (13). However, the increase in insulin sensitivity was limited, as diagnoses of T2D and other co-morbidities excluded many participants from the study. In addition, different ethnic groups showed different ranges of results, and individuals with a higher genetic risk for IR were less

likely to improve after a year (13). In a different study, nutrition education was effective at decreasing IR among pregnant mothers at risk of developing IR and subsequently gestational diabetes mellitus (GDM), while weight control had no effect and FPG concentrations did not decrease (10). In this case, a nutrition-focused education intervention was more effective than weight management to decrease IR and GDM, indicating the impact nutritional choices can have on metabolic health (10). Understanding the etiology of insulin resistance is necessary for successful development of therapies designed to prevent, treat, and reverse insulin resistance and its many related comorbidities.

Impairments to Metabolic Flexibility Affect Mitochondrial Metabolism

Alterations to mitochondrial metabolism are implicated as a contributor to the development of insulin resistance and progression to T2D. Normal energy metabolism is flexible, resulting in coordinated shifts between fatty acid and glucose oxidation as needed for physiological states. This metabolic flexibility enables fuel selection in transition states, and is required to appropriately meet energy demands during exercise (18). In lean patients, mitochondria that are metabolically flexible coordinate the shifts between available substrates depending on physiological need. Insulin plays a major role in this, as it coordinates the storage or utilization of fuel throughout the body. Insulin resistance results in inappropriate nutrient partitioning, as cells fail to respond to normal levels of insulin signaling (18). Metabolic flexibility has been shown to improve with exercise and prevent insulin resistance, but other results have shown that insulin resistance can be present if mitochondrial function is unaffected (30). Impaired metabolic flexibility is seen in individuals with obesity-related cardiometabolic diseases, and electron microscopy has shown skeletal muscle mitochondria are significantly smaller in T2D and obese subjects than in lean subjects, indicating an impaired capacity for

bioenergetics (14). Other investigators have attributed decreases in mitochondrial respiration between T2D and lean patients to lower numbers of mitochondrial content, not to dysfunction driven by insulin resistance (3). Dysregulated fatty acid metabolism, lipid accumulation, and changes in mitochondrial energetics may also lead to insulin resistance, which begins when target tissues fail to respond to insulin, generally resulting in an increase in insulin secretion from the pancreas due to the blunted response to the initial release of insulin (11), (5). As such, there is debate over if perturbation in mitochondrial function is a cause, consequence, or contributor to insulin resistance and risk of T2D (9).

High-fat diets (HFD) have been shown to decrease sensitivity to insulin and contribute to mitochondrial dysfunction, and lipid accumulation in insulin-target tissues is strongly associated with the development of insulin resistance as it is known to reduce insulin-stimulated glucose uptake. This accumulation may be caused in part by the reduced capacity of the cell to oxidize fat, leading many to theorize that lower levels of oxidative phosphorylation (OxPhos) in mitochondria may be the cause of insulin resistance (6). Mitochondrial function has been shown to be impaired, and insulin resistance present, even in non-diabetic lean offspring of diabetic parents (23). In these offspring, baseline mitochondrial OxPhos activity is decreased, skeletal muscle mitochondrial density and number are reduced, and insulin-stimulated non-oxidative glucose metabolism rates are lower, while intramyocellular lipid (IMCL) content is higher (23). In mouse studies, HFD mice showed changes in mitochondrial proteins associated with the citric acid cycle (TCA), OxPhos, and lipid metabolism. In human muscle, mitochondrial content was reduced in T2D and obese patients (26).

Skeletal muscle mitochondria are integral for shifting between physiological states as the body metabolizes fuel, since skeletal muscle is the main source of postprandial glucose storage.

In this process, mitochondria utilize carbon intermediates obtained from fatty acids, glucose, and amino acids to produce ATP - the energetic 'currency' of the cell - via the TCA cycle, OxPhos, and electron transport. This process consumes oxygen, requires many different cellular mechanisms to interact, and is carefully coordinated and regulated. A decrease in mitochondrial functionality in skeletal muscle may indicate the onset of insulin resistance, especially in obese patients (11).

Mitochondrial Dysfunction is Key in Skeletal Muscle

Skeletal muscle is a principal determinant of whole-body glucose metabolism and displays remarkable capacity for alterations in mitochondrial metabolism, thereby playing a key role in the development of insulin resistance and metabolic inflexibility. The skeletal muscle of obese humans is characterized by the inability to respond to alterations in substrate availability, thus demonstrating decreased metabolic flexibility (4). Mitochondrial dysfunction may arise as a consequence of muscular fat accumulation, inhibiting metabolic shifts and contributing to the onset of insulin resistance by further favoring lipid accumulation. Overnutrition has an obvious link to insulin resistance through HFD, but can also include excess protein intake and excess circulating amino acids, which have been clearly linked to the development of insulin resistance (23). However, it is unknown if this excess also modulates mitochondrial biology in skeletal muscle (23). Overall, patients with T2D show lower respiratory activity and lower oxygen flux in skeletal muscle, resulting in energy dysfunction. This dysfunction may be because these patients have fewer mitochondria overall, or because their function is limited or inhibited to an extent (3), (5).

Reactive Oxygen Species (ROS) and oxidative stress are also involved in the etiology of insulin resistance, mitochondrial dysfunction, and subsequent development of T2D, which is

shown primarily in skeletal muscle tissue. Fatty acid oxidation generates more ROS within the mitochondria than glycolysis, and skeletal muscle generates ROS during both exercise and rest periods (5). In mouse and rat models made insulin resistant through high-fat diets, ROS produced via fatty acid oxidation during states of hyperlipidemia is indicated to further promote lipid accumulation as well as alterations to and inhibition of the mitochondria (5). Mitochondrial levels of H_2O_2 production may play a role in insulin resistance, as it can stimulate or inhibit insulin signaling depending on the concentration and location of H_2O_2 production relative to insulin signaling components (5).

Mitochondrial respiration in response to different substrates varies, as shown by the changes in mitochondrial capacity after exposure to fatty acids, for example (30). However, the effect of fatty acid oxidation on the development of insulin resistance is debated (11). Some argue that mitochondrial capacity is not sufficient for high levels of nutrients, or that ATP-consuming processes effectively limit mitochondrial capacity in response to the presence of certain substrates, such as palmitate (22). Obese human cells have been shown to be inflexible in response to lipid exposure, and other experiments with fresh permeabilized skeletal muscle fibers from obese T2D patients have shown decreased state 3 respiration in presence of substrates such as malate, pyruvate, glutamate, and succinate, but not to palmitoyl carnitine and malate. This indicates a difference in the function of different complexes and respiratory activity supported by glutaminolysis, glycolysis, and fatty acid oxidation, which is impacted by insulin resistance and T2D (4). In cellular models, individual substrates can be added in varying sequences. This allows for the evaluation of each substrate's effect on the metabolic system, as well as an assessment of mitochondrial capacity and respiratory control. An examination of metabolism on an individual

substrate basis within a model system allows for the precise dissection of each nutrient's contribution to respiration, and could allow for detection of initial mitochondrial dysfunction.

Investigating Metabolism in Model Systems

The L6 rat myoblast cell line is frequently used to investigate metabolism and to examine mechanisms of insulin resistance in skeletal muscle, as it provides a model system to repeatedly inspect respiratory control, thereby avoiding the need for multiple tissue samples from animals or humans. It is relatively straightforward to replicate disease progression in L6 cells, and a previous study has indicated that respiration in L6 cells tends to mirror that of human cells (21). The control of mitochondrial function and overall levels of cellular respiration in L6 rat myoblasts must be understood, as the high prevalence of IR, obesity, and related diseases requires a greater understanding of the regulation of skeletal muscle metabolism, particularly regarding the ability of the skeletal muscle to oxidize available substrates and produce energy. A systematic evaluation of respiratory control in L6 rat myoblasts will help advance understanding of the contribution of individual metabolic substrates, such as lipids, to mitochondrial respiration. Such information will address a gap in knowledge regarding the ability of mitochondria to efficiently oxidize excess substrates, which are associated with obesity and the development of insulin resistance.

Identifying Respiratory Control in the Mitochondria

The purpose of this investigation was to characterize the intrinsic mitochondrial metabolism and determine the control of mitochondrial respiration in L6 myoblasts using high-resolution respirometry. Changes in mitochondrial function in L6 myoblasts due to the addition of specific substrates were analyzed using high-resolution respirometry in combination with Substrate-Uncoupler-Inhibitor-Titration (SUIT) protocols to establish measures of cellular

respiration and determine the contribution of specific substrates to changes in respiration. We hypothesized that substrates related to lipid oxidation will exert less control over respiration than non-lipid substrates, indicated by lower oxygen consumption. Understanding the contribution of individual metabolic substrates to cellular respiration will help to elucidate the ability of mitochondria to efficiently oxidize excess substrates. It is thought that mitochondrial impairment could contribute to the onset of insulin resistance, so to draw conclusions from metabolic data to effectively approach treatment for obesity, insulin resistance, and related diseases, a baseline for respiration and respiratory control in model systems must first be established and understood in order to inform further metabolic studies and analyses of cell processes. Completing this study will identify the metabolic capabilities of the L6 myoblasts when presented with substrates in excess, thereby furthering understanding of mitochondrial metabolism in these cells.

METHODS

Cell Culture and Harvest

We investigated mitochondrial respiratory control and substrate oxidation in cultured muscle cells which are commonly used as a model for skeletal muscle tissue metabolism. L6 rat myoblasts from American Type Culture Collection were cultured in T75 flasks at a humidified 37°C and 5% CO_2 in Dulbecco's Modified Eagle's Medium (DMEM), which included 4.5g/L glucose, 0.584 g/L L-glutamine, 110 mg/L sodium pyruvate, supplemented with 10% fetal bovine serum and 1% antibiotic-antimycotic. Media and reagents used for culture were purchased from Gibco. Cells passed upon reaching 80%-90% confluence. Dulbecco's Phosphate Buffered Saline (DPBS) was used to rinse the myoblasts to eliminate cellular debris and residual media, after which the myoblasts were incubated in 0.25% trypsin-EDTA for 5 minutes. Cells were recovered and the trypsin inactivated with growth media. Cells were pelleted (180 x g for 5 minutes) at room temperature then the supernatant was discarded and cells were suspended in growth media. Cells were distributed into new T75 flasks at ratios of 1:4-8, with no more than 5 passages prior to being harvested for experiments.

When needed for an experiment, cells from four T75 flasks were pelleted at room temperature (180 x g for 5 minutes). Growth media was removed through rinsing and re-suspending the pellets in DPBS. Cells were re-pelleted with centrifugation (180 x g for 5 minutes), then the DPBS was aspirated off. All cell pellets were combined in 1 mL of MiR05 respiration buffer (0.5 mM EGTA, 3 mM $MgCl_2$-$6H_2O$, 60 mM Lactobionic acid, 20 mM taurine, 10 mM KH_2PO4, 20 mM HEPES, 110 mM sucrose, 1 g/L bovine serum albumin). Cells were counted using a hemacytometer then diluted to 4 million cells per mL. Cells used in the GMS and PCM protocols were permeabilized with digitonin prior to being added to the

chambers of the Oxygraph. 250 μL was added to each chamber of the O2k. A total of $1x10^6$ cells were analyzed for respiration in each chamber.

High-resolution Respirometry with the Oxygraph O2k System

Mitochondrial oxygen consumption and ROS production must be quantified to evaluate the effect of metabolic fuels on mitochondrial function and respiratory control and find potential limits to mitochondrial capacity. To quantify respiration, cellular oxygen consumption and concentration was measured using high-resolution respirometry, performed in the Oxygraph O2k system (Oroboros Instruments Corp, Innsbruck Austria). Substrate-Uncoupler-Inhibitor-Titration (SUIT) titration protocols (shown in Tables 1, 2, and 3 below) assessed mitochondrial respiratory control through fatty acid, NADH-, and FADH-linked substrates. Changes to respiration with substrates or inhibitors enabled the evaluation of respiratory control and the function of mitochondrial complexes. Changes in oxygen concentration were continuously recorded and steady-state oxygen fluxes were determined for each respiratory state including oxidative phosphorylation (P), electron system capacity (E), leak respiration (L) and residual oxygen consumption (ROX). Reactive oxygen species production was simultaneously measured using a flourometric analysis of H_2O_2 production.

SUIT Oxygraph O2k Respiration Protocols

We assessed mitochondrial function with three separate protocols. The GMS and PCM protocols were implemented as previously demonstrated by the Translational Metabolism Research Laboratory (19). Reference Protocol 2 (RP2) was developed by Oroboros Instruments Corp. Each protocol examined the impact of assorted substrates on respiration in a different manner, as described below. This allowed for the separation of pathways that contribute to respiration so their impact, as well as any potential inhibitory effects a pathway or substrate

could have on respiration, could be determined. Substrates which contribute to the NADH-linked (N-linked substrates) respiratory pathway, Complex II-linked pathway (S-linked substrates), β-oxidation (F-linked substrates) and CGpDH respiratory pathway (Gp-linked substrates) were all added during the three different protocols in ways that enabled measurement of both their individual and additive contributions to respiration through their separate respiratory pathways to the Q-junction (*Fig. 1*).

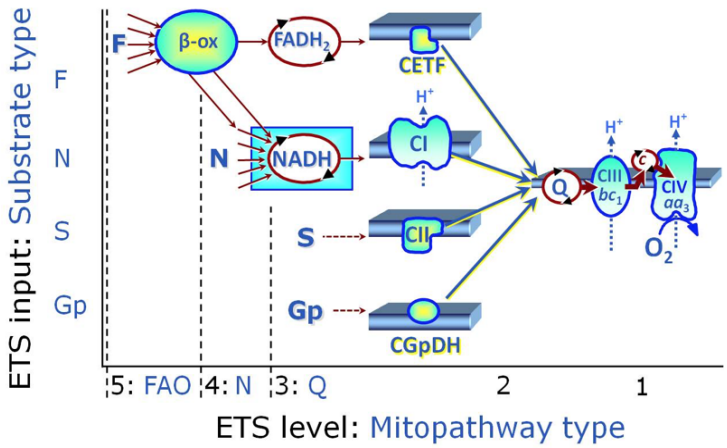

Figure 1: Each respiratory pathway and their substrate inputs, displayed through separation based on how each contributes to the electron transfer system (8).

Glutamate-Malate-Succinate (GMS) Protocol: Citric Acid Cycle-Based Respiration

The GMS Protocol evaluates N- and S-linked substrate-driven respiration in both Complex I and Complex II, respectively. When combined with malate, glutamate results in higher levels of respiration than either would alone. Provision of malate also reduces feedback inhibition, as in the PCM protocol (27). Saturation with succinate enables measurement of Complex II contribution to respiration, both in conjunction with N-linked substrates and alone when rotenone is added, which inhibits Complex I. Glutamate also contributes to the malate-aspartate shuttle. Cellular ROS production was measured through the emission of H_2O_2, which was measured using continuous flurometric detection of resorufin (Amplex® Red) in the

presence of horseradish peroxidase and superoxide dismutase. The detailed sequence for this protocol is displayed in Table 1, and an example tracing of the GMS protocol run is shown in Figure 5.

Palmitoyl-Carnitine-Malate (PCM) Protocol: Fatty Acid-Supported Respiration

The PCM protocol evaluates respiration driven by fatty acid oxidation through Complex I and CETF. It relies on the use of palmitoyl-L-carnitine to bypass the possible rate-limiting step in β-oxidation, and malate to support the progression of respiration by reducing feedback inhibition of pyruvate dehydrogenase (24), (27). Complex II is fed only through endogenous succinate, which contributes little to nothing to respiration, as in permeabilized cells it is unlikely sufficient amounts of succinate to drive respiration will be present. Cellular ROS production was measured as the production of H_2O_2 as measured using continuous flurometric detection of resorufin (Amplex® Red) in the presence of horseradish peroxidase and superoxide dismutase. The detailed sequence for this protocol is displayed in Table 2, and an example tracing of the PCM protocol run is shown in Figure 6.

Reference Protocol 2 (RP2): Sequential Substrate Respiration

The sequential steps of the RP2 protocol, designed by the creators of the Oxygraph O2k, enabled quantification of the additive effects of different substrates on oxidative phosphorylation, allowing us to examine the contribution from each pathway to overall mitochondrial metabolism. It includes N-, S-, F-, and Gp-linked substrates which feed into each complex, and inhibitors allowing for quantification of each complex's contribution to respiration during separate respiratory states. The initial addition of a low concentration of malate prevents inhibition of respiration driven by subsequent substrates, and high malate ensures respiration is not limited. Glycerol 3-phosphate contributes to respiration as well, feeding electrons into the Q-

junction from cGDPH (17). Digitonin is added to the chambers of the Oxygraph to ensure permeabilisation. The detailed sequence for this protocol is displayed in Table 3, and an example tracing of the RP2 protocol run is shown in Figure 7.

Statistical Analysis

Mitochondrial respiration was compared as the change in oxygen consumption between respiratory states during the SUIT protocol. Changes to respiratory control were analyzed by repeated measure one-way ANOVAs and paired t-test with significance at $p=0.05$. Data are presented as mean ±, standard deviation from $n=6$ per protocol. Statistical analysis and graph construction were performed in Prism v.6 (GraphPad Software Inc., La Jolla, CA).

RESULTS

Glutamate-Malate-Succinate (GMS) Protocol

The GMS protocol assesses the roles Complex I and Complex II play in respiration through the addition of N- and S-linked substrates. These substrates contribute to the TCA cycle through simple single step reactions, enabling the evaluation of the overall system's respiratory control and the contribution of each complex to respiration.

OxPhos occurred first in ADP-saturated conditions with N-linked Glutamate+Malate, and then increased after the addition of S-linked succinate (*p=0.002, GM vs. Succ., Fig. 2A*). The addition of Cytochrome C tests the integrity of the mitochondrial membranes. Low changes (<10%) in respiration indicate that they are still intact (*p=>0.99 between Succ. and Cyt. C., mean difference <0.06 JO_2, Fig. 2A)*.

Oligomycin inhibits Complex IV (ATP Synthase), stopping ATP production. The oxygen consumed during this time is consumed due to electron leak from the intermembrane space into the matrix. Leak comprised 13% of total oxygen consumption, and was not significantly different from ROX *(p=0.23)*. Oxygen consumption due to Leak electron flow is driven by the large membrane potential present in the mitochondria.

FCCP, an uncoupler, is added to determine the oxygen consumption representing the maximal capacity of the electron transfer system (ETS), powered by N+S-linked substrates. ETS-driven oxygen consumption significantly exceeded that of OxPhos once the uncoupler was added *(p= 0.01 between Succ. and FCCP, Fig. 2A*), indicating that N- and S-linked oxidative phosphorylation does not enable maximal electron transfer despite their separate contributions to the Q-junction.

Respiratory control compares oxidative phosphorylation and the capacity of the electron transfer system to identify potential limitations in respiration (*Fig. 2B*). Oxidative phosphorylation with N+S-linked substrates accounted for 75% of maximal non-coupled oxygen consumption, indicating that oxidative phosphorylation was not limited by the electron transfer system capacity, and exerted control over respiration.

The addition of rotenone inhibits Complex I, separating its contribution to respiration from that of Complex II (*p=<0.0001 between FCCP and rotenone, Fig. 2A*). Thus, the contribution of each complex to maximal electron transfer within the mitochondria can be quantified, as shown in *Fig. 2C*.

Comparing the capacities of each respiratory state can identify each state's contribution to respiration. S-linked respiration comprised 54% of total (N- and S-linked) electron transfer *(p=<0.0001 between FCCP and rotenone, Fig. 2C)*. N-linked substrates glutamate and malate comprised only 47% of oxidative phosphorylation within the GMS protocol *(Fig. 2D, p=0.0002)*, indicating the larger contribution to respiration succinate may have, relative to N-linked substrates.

The addition of Antimycin A inhibits electron transfer, allowing for measurement of residual oxygen consumption (ROX). ROX was not different from baseline, indicating little oxygen was consumed for use in background cellular functions unrelated to respiration.

ROS emission during oxidative phosphorylation was significantly different from basal overall (*p=<0.0001 for cells vs. GM and cells vs. Succ., Fig. 2E*). H_2O_2 emissions, measured with fluorometric analysis before the addition of Cytochrome C, increased with the addition of glutamate+malate and succinate. The increase in respiration after the addition of glutamate+malate explain the initial increase in H_2O_2 emissions, but H_2O_2 levels were

significantly different between N- and S-linked substrate oxidation as well (*Fig. 2E, p=0.02*). However, oxygen consumption increased by 16.97 JO_2 (mean difference) between basal cellular respiration and respiration after the addition of glutamate+malate, but emission levels increased by 0.307 JH_2O_2 (mean difference). The H_2O_2 emitted after the addition of succinate increased by only 0.028 JH_2O_2 (mean difference) from emission levels reached with glutamate+malate, despite an increase in oxygen consumption of 18.96 JO_2 (mean difference).

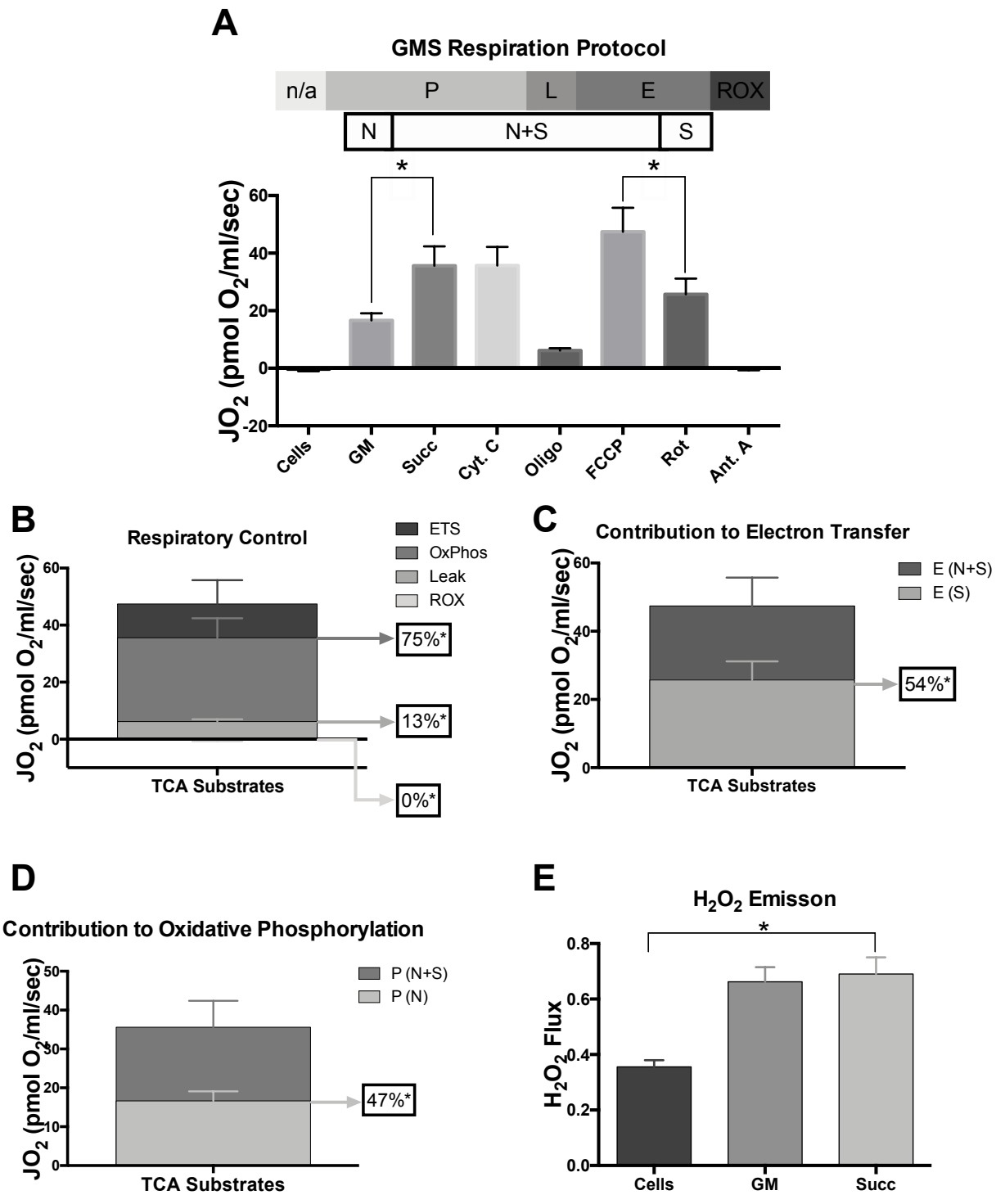

Figure 2: Cellular respiration during the Glutamate-Malate-Succinate (GMS) protocol. The protocol as a whole, displaying levels of respiration during each respiratory state (oxidative phosphorylation (P), electron transfer system capacity (E), leak respiration (L) and residual oxygen consumption (ROX)) and after the addition of each substrate, which are N- or S-linked as noted (A). Respiratory control in the mitochondria was assessed by separating oxygen consumption during each respiratory state as a percentage of oxygen consumption (JO_2) during uncoupled electron transfer, representing maximum capacity (B). The contribution of N- and S- linked and of only S-linked substrates to

uncoupled electron transfer was assessed by measuring the oxygen consumption after the addition of FCCP and then after the addition of rotenone, which inhibits Complex I (C). N- and S- linked and only N-linked substrates drive oxidative phosphorylation (OxPhos), although not equally, with N-linked glutamate (G) and malate (M) comprising 47% of total OxPhos (D). H_2O_2 emission was measured at baseline, after N-linked substrates were added, and after S-linked succinate (Succ) was added to quantify effects of each on ROS production (JH_2O_2, E). Respiration was performed in duplicate on 1x10^6 L6 myoblasts added per 2 mL Oxygraph chamber. Data are mean (SD) from n=6. Asterisks indicate significant difference. Substrate abbreviations not noted previously include oligo = oligomycin, Cyt. C = Cytochrome C, rot = rotenone, and Ant. A = antimycin A.

Palmitoyl-Carnitine-Malate (PCM) Protocol

The PCM protocol assesses respiration driven by fatty acid oxidation with the addition of F-linked palmitoyl-L-carnitine and N-linked malate. Oxygen consumption significantly increased after the addition of these substrates (*p=<0.0001 between Cells and PM*), and the mitochondrial membranes remained intact, as indicated with the addition of Cytochrome C (*p=>0.99, mean difference between PM and Cyt. C =0.09, Fig. 3A*).

ROX accounted for 2% of total oxygen consumption and Leak comprised 13% of total oxygen consumption. However, no significant difference between oxygen consumption after the addition of palmitoyl-L-carnitine and malate and maximal ETS capacity was present (*p=0.37, Fig. 3A*), as oxidative phosphorylation reached 88% of the maximal electron transfer system capacity (*Fig. 3B*).

H_2O_2 emission during Leak was significantly higher than basal (*p=0.0004*), but was highest during OxPhos-driven respiration of palmitoyl-L-carnitine *(p=<0.02 between Leak and PM, Fig. 3C)*.

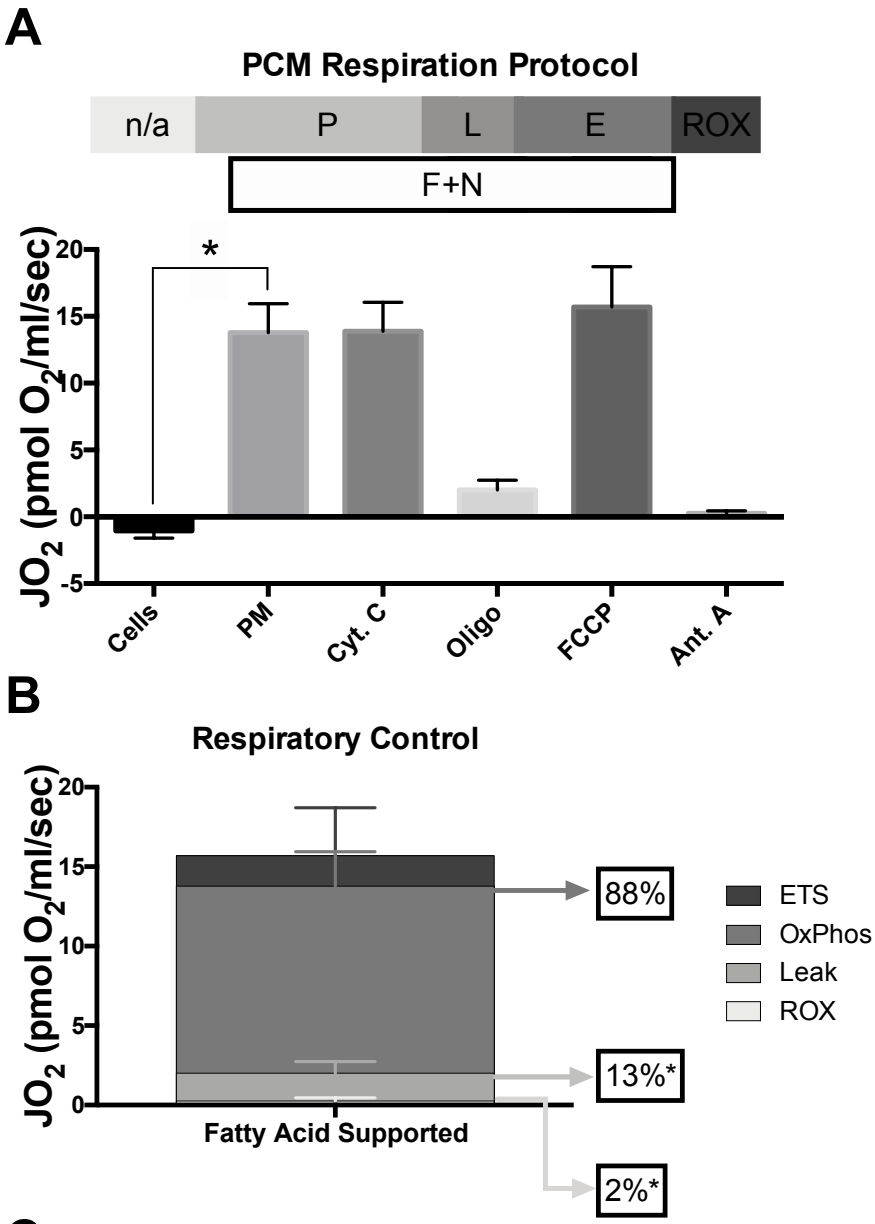
A
PCM Respiration Protocol
n/a
P
L
E
ROX
F+N
*
JO2 (pmol O2/ml/sec)
20
15
10
5
0
-5
Cells
PM
Cyt. C
Oligo
FCCP
Ant. A
B
Respiratory Control
JO2 (pmol O2/ml/sec)
88%
13%*
2%*
ETS
OxPhos
Leak
ROX
Fatty Acid Supported
C
H2O2 Emisson
*
H2O2 Flux
0.8
0.6
0.4
0.2
0.0
Cells
Leak
PM

Figure 3: Cellular respiration during the PCM protocol. The protocol sequence and oxygen consumption during each respiration state after the addition of each substrate, which are F+N-linked as noted (A). Respiration control represented as a percentage of oxygen consumption during each respiratory state (B). ROS production was measured after the addition of the cells to the Oxygraph, during Leak, and during oxidative phosphorylation (C). Respiration was performed in duplicate on 1x10^6 L6 myoblasts added per 2 mL Oxygraph chamber. Data are mean (SD) from n=6. Asterisks indicate significant difference. Substrate abbreviations not noted previously include PM = palmitoyl-L-carnitine + malate.

Reference Protocol Two (RP2)

RP2 was designed as a protocol through which respiration in any cell type or tissue could be examined and compared in a standardized fashion. It assesses the additive influence of substrates on respiration by incorporating aspects of the GMS and PCM protocols, such as N-, S- and F-linked substrates, and introducing Gp-linked substrates as well. This maximizes the inputs for electron transfer by incorporating fatty acid oxidation, Complex I, Complex II, and cGPDH as contributors of electrons to the Q-junction (*Fig. 4A*).

Oxygen consumption driven by F-linked octanoyl carnitine was not significantly different from routine respiration (R), but it comprised 31% of total oxidative phosphorylation *(p=0.048 between F-linked OxPhos and OxPhos driven by all substrates, Fig. 4B)*. The addition of N-linked highly concentrated malate led to a significant increase in oxygen consumption (*p=<0.0001 between octinoyl carnitine and high malate, Fig. 4A*). The sequential additions of N-linked pyruvate and glutamate did not significantly increase oxygen consumption beyond the level reached previously with high malate. Despite this lack of increase, F- and N-linked substrate oxidation provided 94% of total oxidative phosphorylation (*p=0.96 between F- and N-linked substrate-driven OxPhos and OxPhos driven by all substrates, Fig. 4B*). The additions of S-linked succinate and Gp-linked glycerol-3-phosphate also failed to stimulate further increases in oxygen consumption, indicating possible saturation and/or inhibition of OxPhos.

Despite their small contributions to oxidative phosphorylation, when mitochondria were uncoupled with FCCP and rotenone was added to inhibit Complex I, S-linked succinate and Gp-linked glycerol-3-phosphate contributed 60% of the total electron transfer capacity measured through Complex II and cGPDH, respectively *(p=0.03 between S- and Gp-linked substrate-driven electron transfer and electron transfer driven by all substrates, Fig. 4C)*.

Oxygen consumed when mitochondria were uncoupled was significantly higher than during oxidative phosphorylation (*Fig. 4D*), representing excess capacity of the electron transfer system. Oxidative phosphorylation was lower, at about 55% of electron transfer system capacity *(p=0.04 for OxPhos vs. total oxygen consumption during electron transfer)*, indicating the control over respiration was driven by oxidative phosphorylation, and not limited by ETS capacity.

Each protocol resulted in significant differences in levels of maximal electron transfer capacity (*Fig. 4E*). However, despite the additional substrates provided, significantly different levels of oxygen were not consumed by the cells during oxidative phosphorylation, whether the cells were provided with the substrates listed in the GMS protocol or RP2. The oxygen consumed by cells did differ from consumption levels during the GMS and RP2 protocols when cells were exposed to the substrates in the PCM protocol (*p=0.01 for PCM vs. GMS and PCM vs. RP2*). ROX-driven oxygen consumption was not significantly different between all protocols. Overall, the three protocols indicate that respiration is controlled at the level of oxidative phosphorylation, not by the capacity of the electron transfer system.

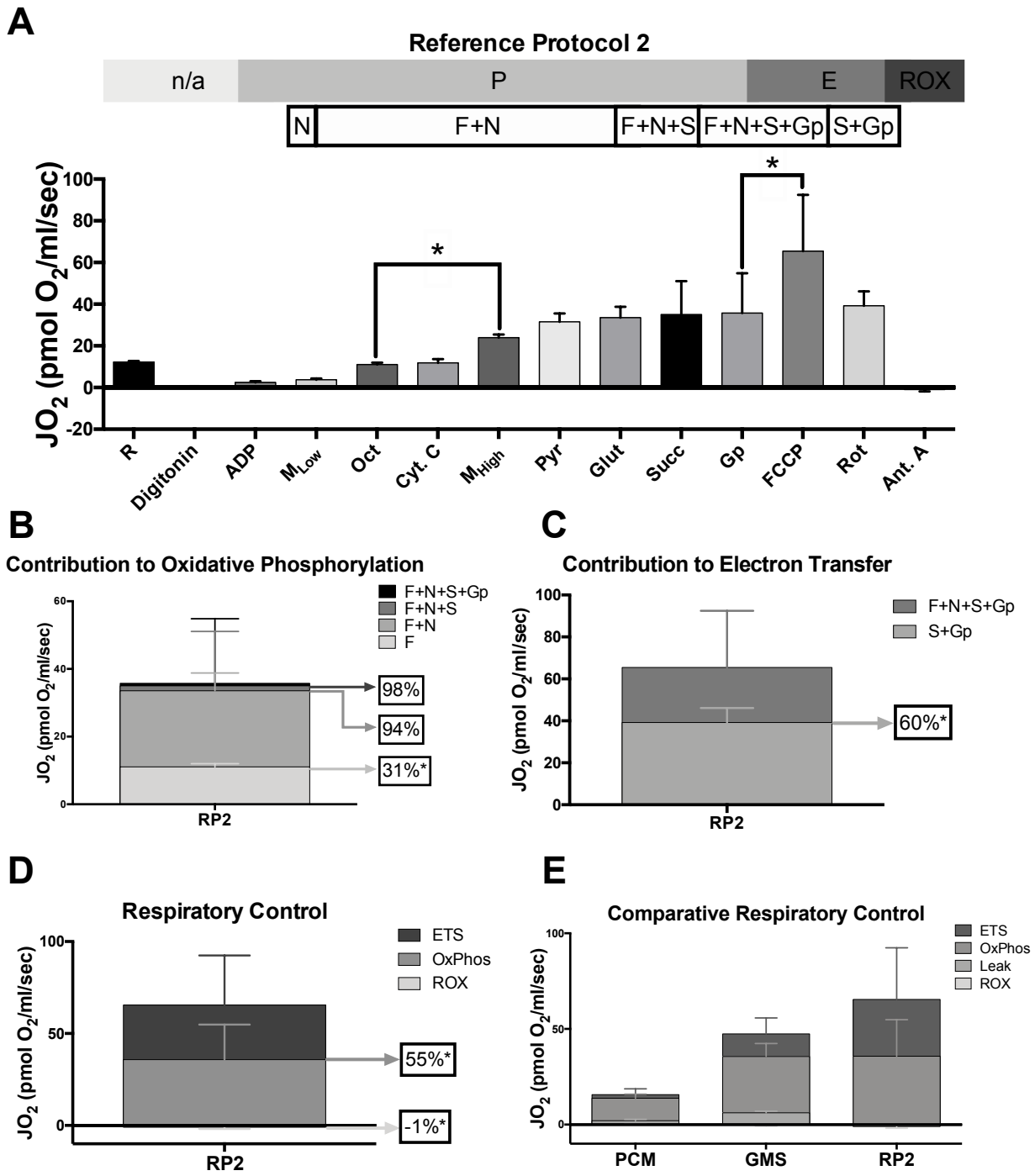

Figure 4: Cellular respiration during RP2. The rates of oxygen consumption after each sequential addition in the protocol are shown based on respiratory state, after the addition of each substrate, which are F-, N-, S- or Gp-linked as noted (A). The cumulative contributions of each type of substrate are shown as a percentage of oxygen consumption during oxidative phosphorylation to evaluate the effect of each type of substrate (B). The contribution of F-, N-, S-, and Gp-linked substrates to maximal electron transfer was separated into just that of S- and Gp-linked substrates with the addition of rotenone (C). Respiratory control as a percentage of maximum capacity was shown for each respiratory state, although Leak could not be measured in the RP2 protocol (D). Each protocol's amount of respiratory control is shown, illustrating the differences in respiration, respiratory capacity, and respiratory control between protocols (E). Respiration was performed in duplicate on 1x10^6 L6 myoblasts added per 2 mL Oxygraph

chamber. Data are mean (SD) from n=6. Asterisks indicate significant difference. Substrate abbreviations not noted previously include R = routine respiration, M_{Low} = low concentration malate, Oct = octinoyl carnitine, M_{High} = high concentration malate, Pyr = pyruvate, Glut = glutamate, and Gp = glycerol-3-phosphate.

DISCUSSION

The purpose of this study was to characterize the intrinsic mitochondrial metabolism of the L6 rat myoblasts with high resolution respirometry. The respiratory control of different substrates (F-, N-, S- and Gp-linked) may have implications for further understanding of respiration in human skeletal muscle and its relation to the regulation of insulin sensitivity. L6 rat myoblasts are a commonly used model system for these studies despite their respiratory control not yet having been well characterized. Respiration was quantified through measurements of oxygen consumption in response to the addition of substrates that contributed electrons to the Q-junction through the mitochondrial complexes. Inhibitors were used to isolate the individual impacts of the complexes on respiration, and potentially identify limitations on respiration within the mitochondria.

Respiratory Control Varied Between Each Protocol

The use of three different SUIT protocols was intended to distinguish aspects of respiration in response to different substrates, including the additive effects substrate additions could have on respiration. The N- and S-linked substrates in the GMS protocol only required single step reactions to enter the TCA cycle, yet the GMS protocol did not include other contributing pathways (such as lipids). Oxygen consumption during the GMS protocol did not reach the same level of oxygen consumption as was reached with RP2 when the mitochondria were uncoupled. This may indicate the presence of a limiting factor during the GMS protocol, or simply the greater mitochondrial capacity possible when more substrates, linked to additional respiratory pathways, are provided, as in RP2. Fatty acid-supported oxidation (measured in the PCM protocol) resulted in rates of oxidative phosphorylation closest to maximal electron transfer capacity, but F-linked substrates alone led to lower respiration rates than were reached when

cells were provided with the substrates included in the GMS and RP2 protocols. The different amounts of oxygen consumption in each protocol indicate respiratory control in L6 myoblasts may be limited by the presence of specific substrates, and that multiple protocols are useful analytical tools for characterizing respiration in any cell line.

Each protocol assessed different aspects of respiration, from the effects of β-oxidation and the TCA cycle on respiration to the impact of combined substrates can have on respiratory control (as is the case *in vivo*). The differences indicate the need for the use of multiple protocols in studies of cellular respiration. We initially believed the RP2 protocol, with multiple substrates contributing to the Q-junction, would maximize respiration in the myoblasts and show the sequential contribution of each type of substrate to respiration. However, oxidative phosphorylation capacity was 55% of the total electron transfer system capacity, and demonstrated an excess capacity for electron transfer rather than oxidative phosphorylation. This excess capacity may be due to inhibition of OxPhos. The change in between oxygen consumption with FCCP to consumption after rotenone was added (inhibiting Complex I) shows that OxPhos may have been inhibited to an extent, potentially by the presence of multiple N-linked substrates. This may be why succinate and glycerol-3-phosphate had little initial effect on respiration (oxygen consumption after the addition of succinate and glycerol-3-phosphate was not significantly different from that reached with N-linked glutamate: *p=>0.9999 between both (Fig.4A)*) but then drove 60% of total electron transfer.

In comparison, in cells exposed to the PCM protocol, F-linked respiration during oxidative phosphorylation was nearly the same as its electron transfer rates. This indicates that F-linked substrates exert a relatively high control of respiration even though total respiration is lower than other N-linked or S-linked substrates. A few possibilities exist for the relative

differences between protocols. For example, the fewer paths to the Q-junction with a single substrate may allow for maximizing oxidative phosphorylation to electron transfer capacity. Additionally, maximal electron transfer may not be significantly elevated within the mitochondria when only in the presence of F-linked substrates.

Oxidative phosphorylation occurred at a lower level than maximal electron transfer when cells were exposed to multiple substrate inputs, as occurred in the GMS protocol. The combination of N- and S-linked substrates contributed multiple inputs to the Q-junction through Complexes I and II, and the GMS protocol highlights the contribution of succinate in respiration as a S-linked substrate (through Complex II). Succinate drove 54% of maximal electron transfer, and increased total levels of oxidative phosphorylation relative to the PCM protocol.

In addition, ROS emissions increased in the presence of succinate from the level emitted in the presence of only glutamate+malate, likely due to higher absolute rates of respiration. Emissions as a function of JO_2 decreased after succinate was added, despite nearly double the amount of oxygen consumed in succinate-driven respiration than in respiration that was driven by glutamate+malate. Overall, higher absolute respiratory rates were seen in cells exposed to the GMS protocol than in those exposed to the PCM protocol, but oxidative phosphorylation during the GMS protocol consumed a lower percentage of the amount of oxygen consumed by the electron transfer system at maximal capacity than in the PCM protocol.

RP2 included the most substrates and paths to the Q-junction but demonstrated the lowest percentage of oxygen consumed during oxidative phosphorylation, relative to the amount consumed by maximal electron transfer, indicating the presence of a limiting factor. The difference between the level of oxidative phosphorylation achieved in the presence of a significant number of substrates and the maximal electron capacity shown contradicts the

argument that mitochondrial capacity is not sufficient for oxidizing high levels of nutrients (22). The capacity of the mitochondria is shown to go beyond that reached with OxPhos, which indicates an ability to utilize nutrients at higher levels. Evidence of a limiting factor impacting respiration in the RP2 protocol includes the observation that cells exposed to RP2 and GMS protocol had essentially the same rates of oxidative phosphorylation despite the presence of additional substrates in RP2, and greater electron system capacity measured during RP2 (*Fig. 4E*). This is further shown by the low initial impact of succinate and glycerol-3-phosphate on respiration, which indicates high substrate availability may be a source of inhibition in metabolism through the overloading of the Q-junction.

Substrate Availability Can Overload the Q-junction and Limit Metabolism

Overnutrition has been previously suggested to lead to metabolic inflexibility over time, impacting the development of insulin resistance. When in a constant nutrient-rich state (a common occurrence thanks to modern eating habits), the mitochondria lose the ability to shift between fuels based on carbon load, instead oxidizing all available substrates at the same time and thereby oversupplying electrons to the Q-junction and increasing ROS generation (18). The RP2 protocol illustrates how sequential substrates may not be truly additive in their effects on respiration and indicate an overloading the Q-junction, which may contribute to the development of a long-term decrease in respiratory control and an eventual increase in metabolic inflexibility.

The differences in the impact the addition of succinate had on respiration are a primary indicator of how respiration can change when mitochondria are potentially overloaded. Depending on the previously added substrates within between the GMS and RP2 protocols, succinate had different effects on respiration. The contribution of succinate to oxidative phosphorylation was a mere 4% of total oxidative phosphorylation in RP2 (*Fig. 4B*), but

combined with glycerol-3-phosphate it made up 60% of maximal electron transfer when the mitochondria were uncoupled (*Fig. 4C*). In the GMS protocol, the contribution of succinate to maximal electron transfer was similar, but the contribution to oxidative phosphorylation was 53% when combined with just N-linked glutamate+malate. This may implicate feedback inhibition of respiration in RP2, potentially stemming from the presence of high concentrations of multiple N-linked substrates.

The similar levels of oxidative phosphorylation in the GMS and RP2 protocols illustrate that adding additional substrates may not stimulate greater phosphorylation in the L6 myoblast cells. However, the additional substrates led to higher rates of oxygen consumption during noncoupled electron transfer, indicating limitations to oxidative phosphorylation were not due to the capacity of the electron transfer system. For example, the combinations of succinate and glycerol-3-phosphate had a greater influence on increasing electron transfer compared to the smaller change in oxidative phosphorylation in the presence of all substrates (*Fig. 4C*). The lack of stimulation of oxidative phosphorylation in the RP2 protocol may be a result of the titration protocol and flooding of the Q-junction by the previously added substrates. The presence of N-linked glutamate, for example, or the overloading of the Q-junction with F- and N-linked substrates may not be optimal for reaching maximal electron transport, even in the presence of other substrates. Such an effect reinforces the idea of a limitation due to the previous addition of F- and N-linked substrates, which consumed 94% of oxygen during oxidative phosphorylation. The differences in respiration and respiratory control between these protocols provide insight into the characterization of mitochondrial metabolism in L6 myoblasts. The overall impact of the contribution of succinate to respiration is clearly significant, but the potential limiting factors present may indicate that a different protocol besides RP2 should be utilized in conjunction with

other protocols to examine respiration in the future. The combined measurements of ROS emissions are important as ROS is implicated in the development of insulin resistance (2).

β-oxidation May Be Near Natural Capacity

Mitochondrial function during fatty acid-supported oxidative phosphorylation came closest to reaching maximal electron transfer capacity. This could have implications for those with high levels of circulating lipids and mitochondrial lipid oxidation with obesity. For example, lower mitochondrial oxidation has been suggested to contribute to the development of insulin resistance with obesity (28). Other reports have indicated that lipid oxidation capacity is increased with obesity (19). In a different study, muscle fibers from obese T2D patients exhibited a decrease in respiration when provided with N-linked malate, pyruvate, glutamate, and S-linked succinate, but did not decrease when exposed to F-linked palmitoyl carnitine and N-linked malate (4). As such, increasing β-oxidation proteins may help increase the oxidative phosphorylation capacity of mitochondria, given that electron transfer system capacity does not seem to be limiting for lipid respiration. On the other hand, β-oxidation capacity in the electron transfer system may be close to its natural limit already. This could be why oxygen consumption as a whole was lower when cells were exposed to the PCM protocol than when exposed to the GMS protocol or RP2. In addition, it may explain why oxygen consumption due to oxidative phosphorylation was not significantly different from the amount of oxygen consumed when the electron transfer system was uncoupled (*Fig. 3B*).

Future Considerations and Limitations

Respiration in other cell models that are used in metabolic research can be characterized to enable comparisons and encourage thoughtful selection when designing methodology for upcoming metabolism-focused cell studies. At the moment, there is no reason to exclude L6

myoblasts from use in such investigations, as there do not appear to be any overt mitochondrial defects in these cells, but there may be a propensity for substrate overload. Because of the overload, alternative protocols should be explored, utilizing high-resolution respirometry to identify substrate additions that will further elucidate the range and limits of mitochondrial metabolism. Furthermore, although the L6 myoblasts were permeabilized with digitonin, these cells were not exposed to insulin at any point. Further studies exploring additional physiological aspects of mitochondrial respiration could reveal potential changes in respiration in response to the multiple signals that are present *in vivo*.

The sequential additions of each substrate may lead one to assume a respective step-wise contribution to respiration with each substrate. This is not an appropriate assumption, and is one we do not make, as each additional increase is merely the minimal increase possible. Interpreting the results of each protocol as the results of sequential substrate consumption means assuming no metabolic shifts occur within the mitochondria. This is incorrect, as similar levels of respiration may be driven by the oxidation of different substrates, and there is no possible way to identify this as it occurs, leaving open the possibility of mitochondrial switching between fuels (18). The RP2 protocol did not allow for measurement of ROS emission (due to interference of the ROS analysis with Cytochrome C) or oxygen consumption due to Leak, limiting the opportunities for comparisons between protocols and analysis of cellular respiratory function during the RP2 protocol. The individual runs of the RP2 protocol also revealed distinct variability in respiration in response to the addition of succinate, despite rates of respiration after the addition of each other substrate holding relatively steady between each individual run. As such, options for comparison and power to detect statistical significance may be limited regarding succinate, but

respiration can still be assessed, and metabolism characterized, across multiple respiratory pathways.

In summary, respiratory activity and control in L6 myoblasts varies in the presence of F-, N-, S-, or Gp-linked substrates, as each substrate, and potentially the order in which they are added, leads to changes in rates of respiration. The intrinsic mitochondrial metabolism in L6 myoblasts appears inhibited by the flooding of multiple paths to the Q-junction, which may limit respiration by impeding OxPhos and minimizing the effect additional substrates can have on increasing rates of respiration once the Q-junction has been flooded. The comparison between oxygen consumption during oxidative phosphorylation and maximal noncoupled electron transfer indicates mitochondrial oxidative capacity in L6 myoblasts is not limited by the electron transfer system. The order in which cells are exposed to different substrates may influence control of mitochondrial respiration. Such considerations are important for understanding the alterations to mitochondrial metabolism that arise during IR, obesity, and chronic metabolic diseases such as T2D.

Appendix

Table 1: Glutamate-Malate-Succinate (GMS) Protocol

Respiration State	Event Substrate Concentrations *Substrate Link*	Description of Pathway and Importance
n/a	**1ce** 1 million cells per chamber *n/a*	1 million cells in Miro5 buffer were added to each Oxygraph chamber after permeabilisation with digitonin.
	H_2O_2 production reagents added 10 µM Amplex® Red, 5 U/ml superoxide dismutase, and 1 U/ml horseradish peroxidase and calibrated using 40 µM injections of H_2O_2 *None*	This enables measurement of H_2O_2 production, allowing for quantification of reactive oxygen species (ROS) production.
L	**1GM** 10 mM glutamate 2 mM malate *N-linked*	N-linked substrates result in the production of NADH, feeding into respiration through Complex I.
P	**1D** 5 mM ADP *N-linked*	Saturating concentrations of ADP maintain oxidative phosphorylation. Glutamate and malate provide electrons through N-linked respiration.
	2S 10 mM succinate *N- and S-linked*	Addition of S-linked substrates contribute electrons through Complex II.
	2c 10 µM cytochrome c *N- and S-linked*	Membrane integrity is tested to verify intact mitochondrial membranes. H_2O_2 measurements cannot proceed after the addition of cytochrome c, since it is incompatible with Amplex red.
L	**3Oligo** 2 µg/ml oligomycin *N- and S-linked*	Inhibition of ATP Synthase (Complex V) prevents oxidative phosphorylation and induces high membrane potential and associated oxygen consumption due to proton leak.
E	**4U** sequential additions of 0.05 mM FCCP to plateau *N- and S-linked*	Disruption of the membrane potential by uncoupling determines the maximal capacity of the electron

		transfer system with N- and S-linked substrates present.
	5Rot 0.5 μM rotenone *S-linked*	Rotenone inhibits Complex I, allowing for measurement of the electron transfer capacity predominantly through S-linked respiration in Complex II.
ROX	**6Ama** 2.5 mM antimycin A *None*	Antimycin A inhibits Complex 3 (Q-junction), preventing the transfer of electrons through the electron transport chain. Only residual oxygen consumption occurs at this point.

Table 2: Palmitoyl-Carnitine-Malate (PCM) Protocol

Respiration State	Event Substrate Concentrations *Substrate Link*	Description of Pathway and Importance
n/a	**1ce** 1 million cells per chamber *None*	1 million cells in Miro5 buffer were added to each Oxygraph chamber after permeabilisation with digitonin
	H_2O_2 production reagents added 10 µM Amplex® Red, 5 U/ml superoxide dismutase, and 1 U/ml horseradish peroxidase and calibrated using 3 injections of H_2O_2 *None*	This enables measurement of H_2O_2 production, allowing for quantification of reactive oxygen species (ROS) production during cellular respiration.
L	**1PM** 0.005 mM palmitoyl-L-carnitine 2 mM malate *F- and N-linked*	Palmitoyl carnitine is an F-linked substrate and malate an N-linked substrate, which feed through Complex I and CETF, and Complex I, respectively, to the Q-junction.
P	**2D** 5 mM ADP *F- and N-linked*	Saturating concentrations of ADP maintain oxidative phosphorylation. Palmitate and malate contribute to respiration through fatty acid oxidation.
	2c 10 µM cytochrome c *F- and N-linked*	Membrane integrity is tested to verify intact mitochondrial membranes. H_2O_2 measurements cannot proceed after the addition of cytochrome c, since it is incompatible with Amplex red.
L	**3Oligo** 2 µg/ml oligomycin *F- and N-linked*	Inhibition of ATP Synthase (Complex V) prevents oxidative phosphorylation and induces high membrane potential and associated oxygen consumption due to proton leak.
E	**4U** Sequential additions of 0.05 mM FCCP to plateau *F- and N-linked*	Disruption of the membrane potential by uncoupling determines the maximal capacity of the electron transfer system with N- and S-linked substrates present.
ROX	**5Ama** 2.5 mM antimycin A *None*	Antimycin A inhibits Complex III (Q-junction), preventing the transfer of electrons through the electron

		transport chain. Only residual oxygen consumption occurs at this point.

Table 3: Reference Protocol 2 (RP2)

Respiration State	Event Substrate Concentrations *Substrate Link*	Description of Pathway and Importance
R	**1ce** 1 million cells per chamber *None*	1 million cells in Miro5 buffer were added to each Oxygraph chamber after permeabilisation with digitonin
n/a	**Digitonin** 1 µL per chamber *None*	Digitonin permeabilizes the cell membrane, enabling substrates to reach the mitochondria.
	1D 5 mM ADP *None*	Saturating concentrations of ADP maintain oxidative phosphorylation.
P	**1M.1** 0.1 mM malate (low) *N-linked*	N-linked malate feeds into respiration through Complex I, traveling to the Q-junction. Low concentrations of malate cannot inhibit other substrates from being measured as they drive respiration, as can occur with high concentrations.
	2Oct 0.5 mM octinoyl carnitine *F- and N-linked*	Fatty acid oxidation (FAO) of F-linked octinoyl carnitine contributes to respiration through CETF and Complex I.
	2c 10 µM cytochrome c *F- and N-linked*	Membrane integrity is tested to verify intact mitochondrial membranes.
	2M2 2 mM malate (high) *F- and N-linked*	N-linked malate feeds into respiration through Complex I. A high concentration is now used to ensure respiration is not limited.
	3P 5 mM pyruvate *F- and N-linked*	N-linked pyruvate feeds into respiration through Complex I.
	4G 10 mM glutamate *F- and N-linked*	N-linked glutamate feeds into respiration through Complex I.
	5S 50 mM succinate *F-, N-, and S-linked*	S-linked succinate contributes electrons to respiration through Complex II.
	6Gp 10 mM glycerol-3-phosphate *F-, N-, S-, and Gp-linked*	Gp-linked substrate contributes electrons that enter the Q-junction from cGPDH to mGPDH. Glycerol-3-phosphate also works within the TCA cycle.

E	**7U** sequential additions of 0.05 mM FCCP to plateau *F-, N-, S-, and Gp-linked*	Disruption of the membrane potential by uncoupling determines the maximal capacity of the electron transfer system with N- and S-linked substrates present.
	8Rot 0.5 μM rotenone *S- and Gp-linked*	Rotenone inhibits Complex I, allowing for measurement of the electron transfer capacity of Complex II with S- and Gp-linked substrates present.
ROX	**9Ama** 2.5 mM antimycin A *None*	Antimycin A inhibits Complex 3 (Q-junction), preventing the transfer of electrons through the electron transport chain. Only residual oxygen consumption occurs at this point.

Figure 5: Sample GMS Oxygraph Tracing

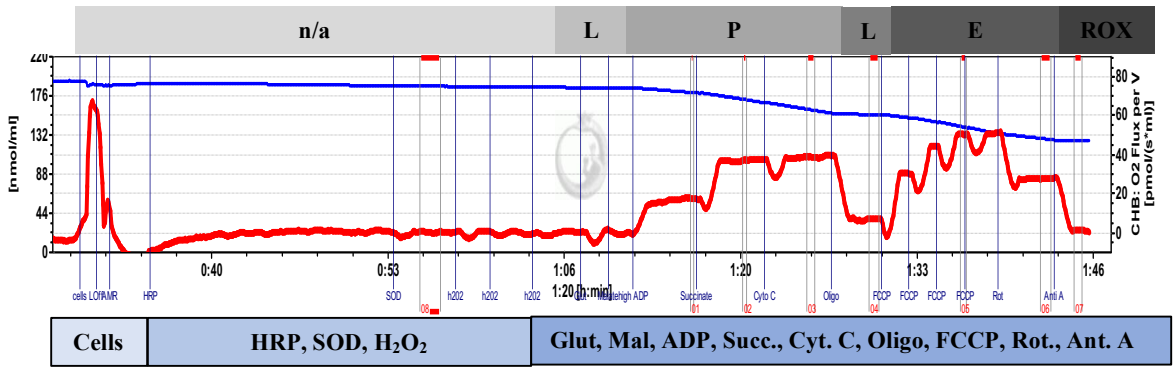

Left axis (blue line): O_2 content [nmol/ml]. Right axis (red line): O_2 Flux per V [pmol/(s*ml)].

Blue vertical lines are substrate additions. Red vertical bars are measurements captured after pertinent substrate additions.

Grayscale boxes above the Oxygraph tracing show respiratory states measured. Blue-scale boxes below the Oxygraph tracing show substrates added.

Figure 6: Sample PCM Oxygraph Tracing

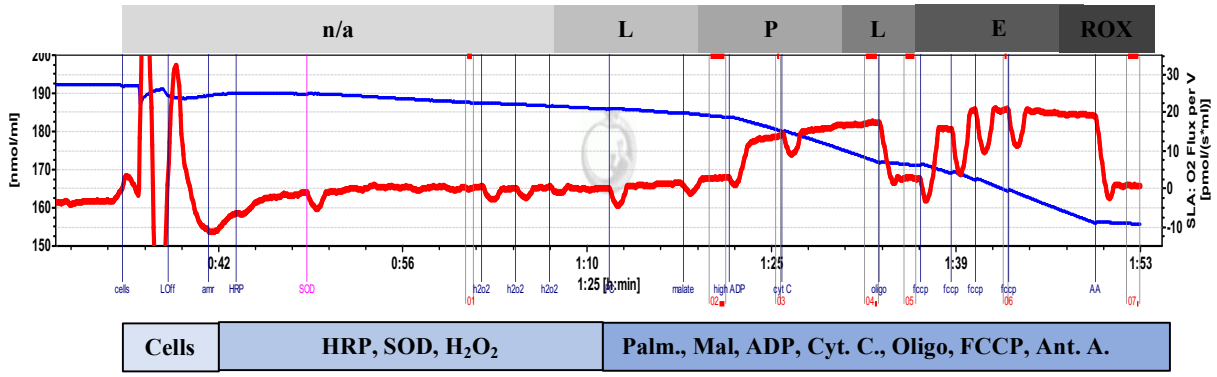

Left axis (blue line): O_2 content [nmol/ml]. Right axis (red line): O_2 Flux per V [pmol/(s*ml)].

Blue vertical lines are substrate additions. Red vertical bars are measurements captured after pertinent substrate additions.

Grayscale boxes above the Oxygraph tracing show respiratory states measured. Blue-scale boxes below the Oxygraph tracing show substrates added.

Figure 7: Sample RP2 Oxygraph Tracing

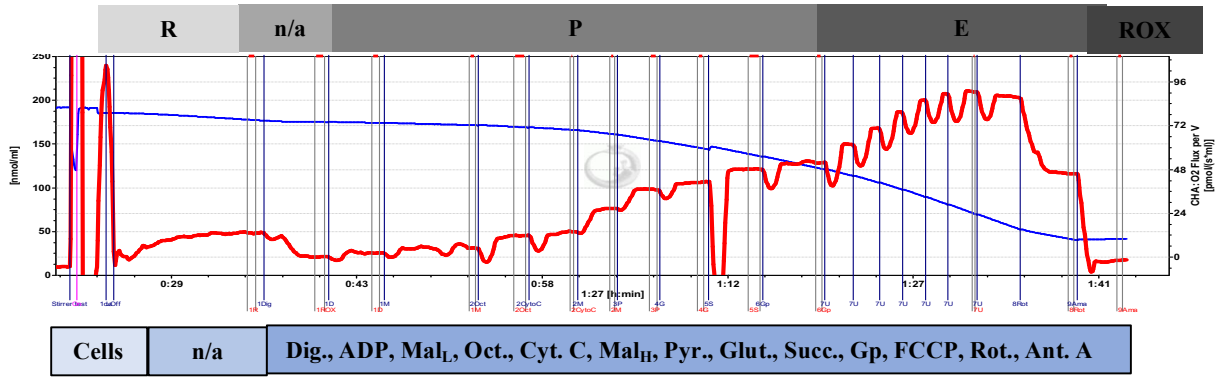

Left axis (blue line): O_2 content [nmol/ml]. Right axis (red line): O_2 Flux per V [pmol/(s*ml)].

Blue vertical lines are substrate additions. Red vertical bars are measurements captured after pertinent substrate additions.

Grayscale boxes above the Oxygraph tracing show respiratory states measured. Blue-scale boxes below the Oxygraph tracing show substrates added.

REFERENCES

1. **American Diabetes A.** Economic Costs of Diabetes in the U.S. in 2017. *Diabetes Care* 41: 917-928, 2018.
2. **Anderson EJ, Lustig ME, Boyle KE, Woodlief TL, Kane DA, Lin CT, Price JW, 3rd, Kang L, Rabinovitch PS, Szeto HH, Houmard JA, Cortright RN, Wasserman DH, and Neufer PD.** Mitochondrial H2O2 emission and cellular redox state link excess fat intake to insulin resistance in both rodents and humans. *J Clin Invest* 119: 573-581, 2009.
3. **Boushel R, Gnaiger E, Schjerling P, Skovbro M, Kraunsoe R, and Dela F.** Patients with type 2 diabetes have normal mitochondrial function in skeletal muscle. *Diabetologia* 50: 790-796, 2007.
4. **Boyle KE, Zheng D, Anderson EJ, Neufer PD, and Houmard JA.** Mitochondrial lipid oxidation is impaired in cultured myotubes from obese humans. *Int J Obes (Lond)* 36: 1025-1031, 2012.
5. **Di Meo S, Iossa S, and Venditti P.** Skeletal muscle insulin resistance: role of mitochondria and other ROS sources. *J Endocrinol* 233: R15-R42, 2017.
6. **Dumas JF, Simard G, Flamment M, Ducluzeau PH, and Ritz P.** Is skeletal muscle mitochondrial dysfunction a cause or an indirect consequence of insulin resistance in humans? *Diabetes Metab* 35: 159-167, 2009.
7. **Finkelstein EA, Fiebelkorn IC, and Guijing W.** National Medical Expenditures Attributable To Overweight And Obesity: How Much, And Who's Paying? *Health Affairs* 22: 8-8, 2003.
8. **Gnaiger E.** Electron transfer-pathway state, edited by FNSGpCIV.jpg S-c. MitoPedia: BioBlast, 2016.
9. **Gonzalez-Franquesa A and Patti ME.** Insulin Resistance and Mitochondrial Dysfunction. *Adv Exp Med Biol* 982: 465-520, 2017.
10. **Goodarzi-Khoigani M, Mahmoodabad SM, Moghadam MB, Nadjarzadeh A, Mardanian F, Fallahzadeh H, and Dadkhah-Tirani A.** Prevention of insulin resistance by dietary intervention among pregnant mothers: A randomized controlled trial. *International Journal of Preventive Medicine* 8: 85, 2017.
11. **Goodpaster BH and Sparks LM.** Metabolic Flexibility in Health and Disease. *Cell Metab* 25: 1027-1036, 2017.
12. **Hardy OT, Czech MP, and Corvera S.** What causes the insulin resistance underlying obesity? *Curr Opin Endocrinol Diabetes Obes* 19: 81-87, 2012.
13. **Hivert MF, Christophi CA, Franks PW, Jablonski KA, Ehrmann DA, Kahn SE, Horton ES, Pollin TI, Mather KJ, Perreault L, Barrett-Connor E, Knowler WC, Florez JC, and Diabetes Prevention Program Research G.** Lifestyle and Metformin Ameliorate Insulin Sensitivity Independently of the Genetic Burden of Established Insulin Resistance Variants in Diabetes Prevention Program Participants. *Diabetes* 65: 520-526, 2016.
14. **Kelley DE, He J, Menshikova EV, and Ritov VB.** Dysfunction of mitochondria in human skeletal muscle in type 2 diabetes. *Diabetes* 51: 2944-2950, 2002.
15. **Kuusisto J, Koivisto K, Mykkanen L, Helkala EL, Vanhanen M, Hanninen T, Kervinen K, Kesaniemi YA, Riekkinen PJ, and Laakso M.** Association between features of the insulin resistance syndrome and alzheimer's disease independently of apolipoprotein e4 phenotype: cross sectional population based study. *Bmj* 315: 1045-1049, 1997.

16. **Lin EA, Barlow GM, and Mathur R.** The Health Burden of Obesity. In: *The Clinician's Guide to the Treatment of Obesity*, 2015, p. 19-42.
17. **Mracek T, Drahota Z, and Houstek J.** The function and the role of the mitochondrial glycerol-3-phosphate dehydrogenase in mammalian tissues. *Biochim Biophys Acta* 1827: 401-410, 2013.
18. **Muoio DM.** Metabolic inflexibility: when mitochondrial indecision leads to metabolic gridlock. *Cell* 159: 1253-1262, 2014.
19. **Newsom SA, Miller BF, Hamilton KL, Ehrlicher SE, Stierwalt HD, and Robinson MM.** Long-term rates of mitochondrial protein synthesis are increased in mouse skeletal muscle with high-fat feeding regardless of insulin-sensitizing treatment. *Am J Physiol Endocrinol Metab* 313: E552-E562, 2017.
20. **Nichols GA and Brown JB.** Higher medical care costs accompany impaired fasting glucose. *Diabetes Care* 28: 2223-2229, 2005.
21. **Nisr RB and Affourtit C.** Insulin acutely improves mitochondrial function of rat and human skeletal muscle by increasing coupling efficiency of oxidative phosphorylation. *Biochim Biophys Acta* 1837: 270-276, 2014.
22. **Nisr RB and Affourtit C.** Palmitate-induced changes in energy demand cause reallocation of ATP supply in rat and human skeletal muscle cells. *Biochim Biophys Acta* 1857: 1403-1411, 2016.
23. **Pagel-Langenickel I, Bao J, Pang L, and Sack MN.** The role of mitochondria in the pathophysiology of skeletal muscle insulin resistance. *Endocr Rev* 31: 25-51, 2010.
24. **Pande SV.** On Rate-controlling Factors of Long Chain Fatty Acid Oxidation. *Journal of Biological Chemistry* 246: 5384-5390, 1971.
25. **Prevention CfDCa.** Prediabetes, edited by National Center for Chronic Disease Prevention and Health Promotion DoDT. Online: Centers for Disease Control and Prevention, 2017.
26. **Sadler NC, Angel TE, Lewis MP, Pederson LM, Chauvigne-Hines LM, Wiedner SD, Zink EM, Smith RD, and Wright AT.** Activity-based protein profiling reveals mitochondrial oxidative enzyme impairment and restoration in diet-induced obese mice. *PLoS One* 7: e47996, 2012.
27. **Salabei JK, Gibb AA, and Hill BG.** Comprehensive measurement of respiratory activity in permeabilized cells using extracellular flux analysis. *Nat Protoc* 9: 421-438, 2014.
28. **Simoneau JA and Kelley DE.** Altered glycolytic and oxidative capacities of skeletal muscle contribute to insulin resistance in NIDDM. *J Appl Physiol (1985)* 83: 166-171, 1997.
29. **Sinaiko AR and Caprio S.** Insulin resistance. *J Pediatr* 161: 11-15, 2012.
30. **Turner N and Heilbronn LK.** Is mitochondrial dysfunction a cause of insulin resistance? *Trends Endocrinol Metab* 19: 324-330, 2008.
31. **Unger J.** *Diabetes Management in Primary Care*: Lippincott Williams & Wilkins, 2013.
32. **Wang YC, McPherson K, Marsh T, Gortmaker SL, and Brown M.** Health and economic burden of the projected obesity trends in the USA and the UK. *Lancet* 378: 815-825, 2011.
33. **Wellman NS and Friedberg B.** Causes and consequences of adult obesity: health, social and economic impacts in the United States. *Asia Pac J Clin Nutr* 11: S705-S709, 2002.